PERGAMON

International Journal of Solids and Structures 39 (2002) 2911–2926

INTERNATIONAL JOURNAL OF SOLIDS and STRUCTURES

www.elsevier.com/locate/ijsolstr

On the post-buckling behavior of bilaterally constrained plates

Herzl Chai

Department of Solid Mechanics, Materials and Systems, Faculty of Engineering, Tel Aviv University, Tel Aviv 69978, Israel

Received 26 November 2001; received in revised form 24 February 2002

Abstract

A combined experimental/analytical effort is carried out to elucidate the post-buckling response of bilaterally constrained columns and plates under monotonically increasing edge displacement. Real-time observations of the outward deformation of the plate via the shadow moire technique facilitate deep insight into the behavior of this class of problems. The lateral constraints lead to a sequential plate snapping process that arise from secondary buckling of a contact zone(s) in the plate. The critical load for mode transition is evaluated systematically as a function of the confining gap, the plate aspect ratio and other system parameters. The results generally exhibit significant scatter that is attributed to the inherent asymmetry of the deformation pattern in such systems. A large-deformation finite element analysis incorporating frictional contact algorithm is used to model the problem. The deformation patterns as well as the critical loads predicted from this analysis generally agree well with the experimental results. A simple analytic expression, based on the linear theory of beams, is developed for the critical loads. The experimental data are found to be well contained by lower and upper bounds from this analysis once the plate surface interacts with the *two* confining planes. The results of this work may serve as a basis for multilaminate design possessing unique mechanical response and superior energy absorption capability. © 2002 Published by Elsevier Science Ltd.

Keywords: Rectangular plates; Buckling; Contact mechanics; Bilateral constraint; Mode transition

1. Introduction

The mechanics of contact between flexible beam or plate elements and a stiff substrate under compression environment is of interest in a variety of engineering applications, including corrugated board panels (Urbanik, 1996; Patel et al., 1997), deep drilling (Wu and Juvkam-Wold, 1995), near-surface delamination (Jones et al., 1985; Chai, 1990a,b; Nilsson and Giannakopoulos, 1995; Shahwan and Waas, 1997; Sekine et al., 2000), sheet metal forming processes (e.g. Gupta et al., 1999; Kim et al., 2000), encased plate sections in civil engineering structures (Wright, 1995), and compliant foil bearing (Roger Ku and Heshmat, 1993). Contact/buckling problems are generally complex, interactive and three dimensional in nature. It is the purpose of this work to develop basic insight into the post-buckling behavior of this class of problems using a combined experimental–analytic/numerical approach.

E-mail address: herzl@eng.tau.ac.il (H. Chai).

0020-7683/02/$ - see front matter © 2002 Published by Elsevier Science Ltd.
PII: S0020-7683(02)00253-6

Simple, analytically tractable one-dimensional contact/buckling configurations are instructive. Chateau and Nguyen (1991) and Adan et al. (1994) show that when a column positioned at a distance from a flat wall is subjected to compression, contact zones may develop leading to buckling mode transition. More recent works dealing with the *bilaterally* constrained column (Chai, 1998; Holmes et al., 1999) have exposed some other unique characteristics of the contact buckling phenomenon, including a sequential mode transition process resulting from secondary buckling in the contact zones, an inherent asymmetry of the deformation pattern, which leads to significant scatter in the buckling mode transition loads, and an interesting form of hysteresis in the load vs. axial displacement curve. In addition to its instructive value, the bilaterally constrained column has also been proposed as a means for evaluating fracture toughness under mixed-mode loading (Kublanov and Bottega, 1995).

Siede (1958) was apparently the first to study contact buckling effects in plates. In his treatment of infinitely long, simply supported plates, Seide found that a rigid lateral constraint may increase the buckling resistance by over 33% relative to the unrestrained plate. Extension of this work to include the effect of foundation stiffness and boundary conditions is given by Shahwan and Waas (1998a,b). Finite size plates under unilateral constraint were treated by a number of authors. Ohatake et al. (1980) studied the evolution of contact region with increasing edge displacement. The effectiveness of the shadow moire technique for exposing the deformation pattern in such structures was demonstrated by Jones et al. (1985) and Comiez et al. (1995). Chai (2000) carried out a systematic study of the unilaterally constrained plate using a combined experimental/numerical approach. The results show that the plate response is characterized by a sequential snapping, the specifics of which are greatly dependant on the aspect ratio of the plate. Unlike for bilaterally constrained column, however, secondary buckling now may occur also in the buckled portion(s) of the plate, similar to the behavior observed for some laterally unconstrained rectangular or circular plates.

The phenomenon of buckling mode transition is central to the mechanics of contact buckling. A great deal of insight into this can be gleaned from studies on common (i.e. laterally unrestrained) plates. Stein (1959) was apparently the first to report this phenomenon in his study of long, rectangular metal plates. Secondary buckling may also occur in axisymmetrically compressed circular plates (e.g. Keller and Reiss, 1958). In this case, the buckles or wrinkles are formed at the plate periphery. Analytic/numeric studies of secondary buckling have been reported by a number of authors, mostly using variational energy principles based on perturbation from a given post-buckling state (e.g. Keller and Reiss, 1958; Nakamura and Uetani, 1979). Such analyses are complex, and generally do not provide information on the new equilibrium state following plate snapping. For a better physical insight into the transition process, a viable experimental program would be beneficial.

In this work we extend our previous plate effort into bilateral constraint. In addition, the bilaterally constrained column is revisited, principally for establishing the merit of analytic bounds for the buckling mode transition loads, and the results are given in Section 2. A systematic study is carried out to elucidate the effects of plate aspect ratio, the gap between the constraining walls and the load level on the plate response. Clamp type boundary support is assumed in order to simulate thin-film delamination problems. The outward plate deformation is observed in real time via the shadow moire technique. A large-strain finite element analysis incorporating a frictional contact algorithm is used to model the plate behavior. The experimental and numerical aspects of the plate problem are reported in Sections 3.1 and 3.2, respectively.

2. One-dimensional model

2.1. Analysis

Let a flat, linearly elastic column of length a, width b, thickness t, Young's modulus E and Poisson's ratio v be constrained by two rigid and frictionless planes such that one plate surface lies on one plane while

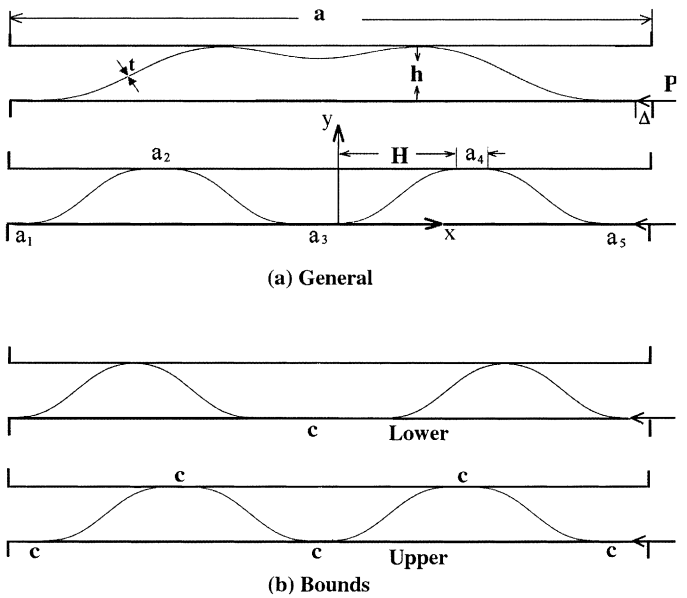

Fig. 1. Stages in the axial compression of a bilaterally constrained column: (a) development of buckling deformation and (b) extreme configurations for $n = 2$.

the other is located at a distance h from the opposing wall (see Fig. 1a). Under axial compression, the column, which is clamped on both ends, buckles. The post-buckling response is studied as a function of the end-to-end shortening, Δ. The fourth-order, linearized differential equation for an Euler beam under axial compression is given by

$$y'''' + k^2 y'' = 0, \quad k^2 \equiv \frac{12P}{Ebt^3}, \tag{1}$$

where a prime sign denotes differentiation with respect to x, y is the lateral deflection and P is the compression force. Following buckling, the column touches the upper wall surface at its midpoint. Upon increasing the load, a line contact develops over the central region of the wall. When the contact length becomes sufficiently large, local buckling ensues (upper sketch in Fig. 1a), leading to a loss of equilibrium and a dynamic transition into a two-buckle configuration (lower part of Fig. 1a). Denote the lengths of the contact segments for this configuration as $a_1, a_2 \ldots, a_{2n+1}$ where n is the total number of buckling waves in the column. Referring to Fig. 1a, the independent boundary conditions for a free-standing segment of a projected length H, taking into account the vanishing of the bending moment along the contact zones, are

$$y(0) = y'(0) = y''(0) = y'(H) = 0, \quad y(H) = h. \tag{2}$$

The solution of this non-homogeneous boundary condition problem is given by

$$\frac{y}{h} = \frac{(2\pi x/H - \sin 2\pi x/H)}{2\pi}, \quad 0 \leqslant x/H \leqslant 1, \tag{3}$$

with the axial force related to the projected length of the free-standing zone according to the following constraint:

$$\frac{kH}{2\pi} = 1. \tag{4}$$

The end shortening is found from the following geometric compatibility condition:

$$\Delta = \varepsilon_0 a + n \int_0^H (y')^2 \, \mathrm{d}x, \tag{5}$$

where ε_0 is the membrane strain, given as

$$\varepsilon_0 = \frac{P}{Ebt}. \tag{6}$$

Substitution of (3) and (6) in (5), and carrying out the integration, the normalized edge displacement is found to be

$$\overline{\Delta} \equiv \frac{3(\Delta/a)}{\pi^2 (t/a)^2} = \frac{ka}{2\pi}\left[\frac{ka}{2\pi} + \frac{9n(h/t)^2}{2\pi^2}\right]. \tag{7}$$

From geometric compatibility

$$\sum_{i=1}^{i=2n+1} a_i + 2nH = a. \tag{8}$$

Multiplying by $k/2\pi$ and making use of (4), one has

$$\frac{k}{2\pi} \sum_{i=1}^{i=2n+1} a_i + 2n = \frac{ka}{2\pi}. \tag{9}$$

2.2. Buckling mode transition

The contact zones spread with increasing Δ until the longest of the flat segments buckles, at which time plate snapping occurs. Subject to the constraint of (9), the individual contact segments may assume arbitrary lengths. This leads to a degree of statistical variations in the onset of local instability. Nevertheless, the load at which mode transition occurs can be bounded. Consider, for demonstrative purposes, the case $n = 2$ (Fig. 1b). The lower limit for mode transition obviously corresponds to a single contact zone, say c. Eq. (9) then reduces to

$$\frac{kc}{2\pi} + 2n = \frac{ka}{2\pi}. \tag{10}$$

On the other hand, the upper limit for mode transition occurs if all the flattened segments are of equal length, say c. Eq. (9) then gives

$$(2n+1)\frac{kc}{2\pi} + 2n = \frac{ka}{2\pi}. \tag{11}$$

Because the flat segment of length c buckles as an Euler column having clamped ends, $kc/2\pi = 1$. Therefore, from (10) and (11), the transition to the next buckling mode is bounded according to

$$1 + 2n \leqslant ka/2\pi \leqslant 1 + 4n. \tag{12}$$

Using (7) and (12), the normalized axial displacement at the transition from n to $n+1$ buckles is bounded as follows:

$$(1+2n)\left[1 + 2n + \frac{9n(h/t)^2}{2\pi^2}\right] \leqslant \overline{\Delta} \leqslant (1+4n)\left[1 + 4n + \frac{9n(h/t)^2}{2\pi^2}\right], \tag{13}$$

where the expressions on the left and right sides of this equation correspond to the lower and upper bounds, respectively.

2.3. Experimental

Compression tests are carried out on bilaterally constrained columns in order to ascertain the applicability of Eq. (13). The test samples are cut from a polycarbonate sheet ($E = 2.3$ GPa, $v = 0.35$) to the dimensions $(b, t, a) = (12, 0.5, 115)$ mm, where b, t and a are the width, thickness and gauge length of the column, in that order. The test fixture and the experimental approach are as described in Chai (1998). The specimen, clamped on all edges, is located between two parallel steel blocks, with one surface resting upon one plane while the other forming an adjustable gap h with the opposite plane. The axial displacement, Δ, is monotonically increased at a slow rate. The axial load, P, and Δ are recorded during the test. The edge of the column is observed in real time with the aid of a video camera.

Figs. 2 and 3 summarize the test results. The variations of the normalized buckling mode transition displacement with the buckling wave number, n, for a given gap value, h (i.e. 0.25 mm), and with h for a given n (i.e. 2), are depicted in Figs. 2 and 3, respectively. The different values for a given parameter depicted in these figures represent repeated tests on the same specimens. The snapping load increases both with n and h, but this effect seems very modest for $h/t < 1$. The data exhibit considerable scatter, but they

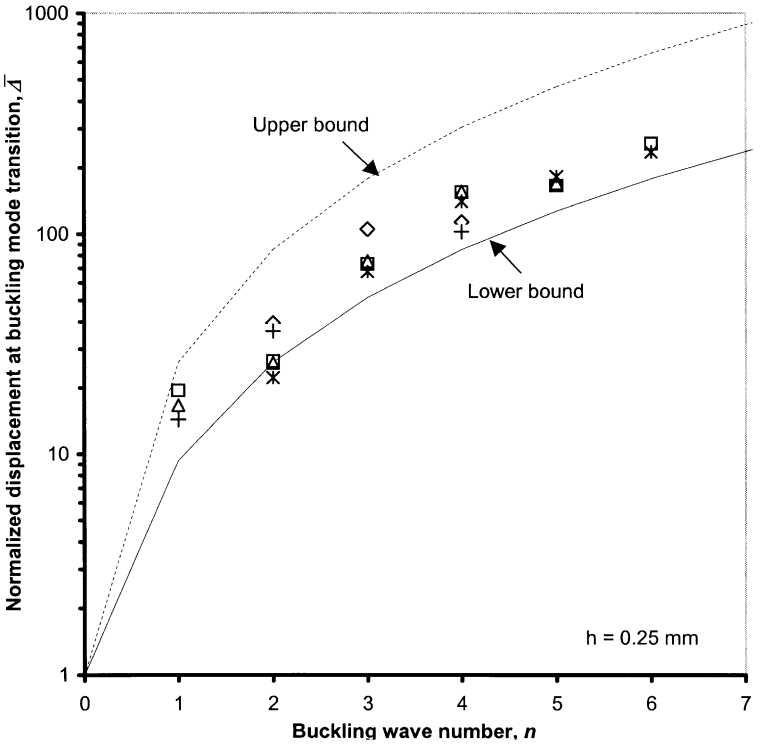

Fig. 2. The normalized axial displacement just after the completion of buckling mode transition, from n to $n + 1$ buckles, as a function of n for a bilaterally constrained column, $h = 0.25$ mm. Different symbols correspond to repeating tests on the same column. Lower and upper bounds are analytic predictions (Eq. (13)).

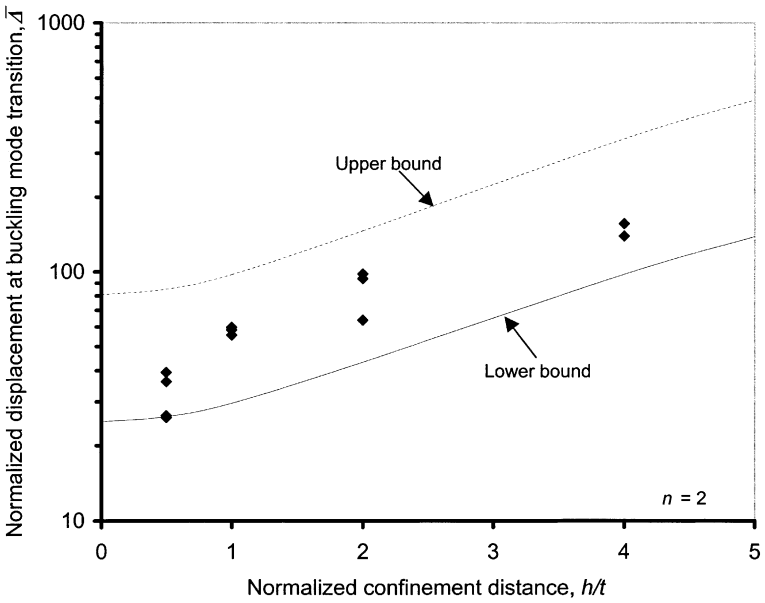

Fig. 3. The normalized axial displacement for buckling mode transition, from $n = 2$ to $n = 3$ buckles, as a function of normalized confinement distance, h/t, for a bilaterally constrained column. Different symbols correspond to repeating tests on the same column. Lower and upper bounds are analytic predictions (Eq. (13)).

are conclusively contained within the analytical bounds given by Eq. (13); note that these curves are meaningful only for integer values of n.

3. The plate problem

Consider a thin rectangular plate of width b, gauge length a and thickness t that is clamped on all four edges. Analogous to the 1-D case, the plate is constrained by two rigid walls positioned at a distance $h + t$ apart, and is subjected to a uniform downward displacement, Δ. It is customary in plate analysis to use the normalized "load" K:

$$K = \frac{12(1-\nu^2)b^2}{\pi^2 t^2}\frac{\Delta}{a} \equiv \frac{4(1-\nu^2)}{R^2}\overline{\Delta}, \tag{14}$$

where $R \equiv a/b$ is the plate aspect ratio and $\overline{\Delta}$ is defined in Eq. (7). The plate behavior can be better understood by considering first the special cases of no constraint and unilateral constraint. For the former, Levy (1942) showed that the buckling deformation has a wavy profile, with the number of buckles increasing while the buckling load decreased as R is increased. When $R = R_0 \approx 1.07$, the deformation changes from a single buckle to two buckles, with $K \approx 10$. This condition is of special significance in the present context since a lateral constraint would delay the emergence of a second buckle. Analysis of the unilateral constraint case (Chai, 2000) showed that for $R > R_0$, the plate buckles into a multitude of waves in quanta of R_0, with the buckling load fixed at a value $K \approx 10$ while n being the smallest closest integer of the ratio R/R_0 (e.g., for $R/R_0 = 1.7$ and 2.3, there will be one and two buckles, respectively). Moreover, because in this range the length of the buckled portion of the plate is less than the plate length, a degree of arbitrariness

in the buckle position occurs. Clearly, this behavior should also characterize the bilaterally constrained plate as long as the outward deformation is less than the confinement distance h. As the load is increased from the buckling state, the buckled plate may interact with the confining plate. This issue is addressed next.

3.1. Experimental

Tests are carried out to elucidate the response of bilaterally constrained, rectangular plates under axial compression. The test samples are cut from polycarbonate sheets to a thickness $t = 0.5$ mm and width $b = 76.2$ mm, with the aspect ratio varying from 1 to 2. A few samples with other dimensions were also tested in order to check the applicability of thin-plate normalizations. Fig. 4 details the testing apparatus. The plate rests against a thick steel block and is further confined by a 25 mm thick, transparent polycarbonate block. The plates are clamped on all four edges, with the bottom edge bolted to the steel block while the upper one is attached to a steel slab that is confined to travel along the vertical direction. The longitudinal edges of the plates are laterally constrained by flat steel bars while they are free to move in the plane of the plate (see Fig. 4b). To reduce geometric imperfections, a high degree of precision in the machining and alignment of all relevant components of the test apparatus is employed.

The outward deformation of the plate is measured via the shadow moire technique (e.g. Kobayashi, 1993). A 6 lines/mm Ronchi ruled glass is bonded to the inner surface of the polycarbonate block. The distance between the plate surface and the glass, h, is adjustable. The moire effect is formed between this grid and its shadow on the deformed, diffusive plate surface. Illumination is achieved using a collimated light beam that is directed at 29° to the plate normal. The sample is viewed in the normal direction, giving a fringe constant, f, of 0.3 mm. The upper edge of the plate is monotonically compressed at a slow rate using a screw driven testing machine (Instron). The axial load, P, applied via a centered steel ball so as to reduce unwanted bending and twisting, and the end shortening, Δ, measured with the aid of an LVDT, are recorded during the tests. The evolving fringe pattern is monitored using a video camera.

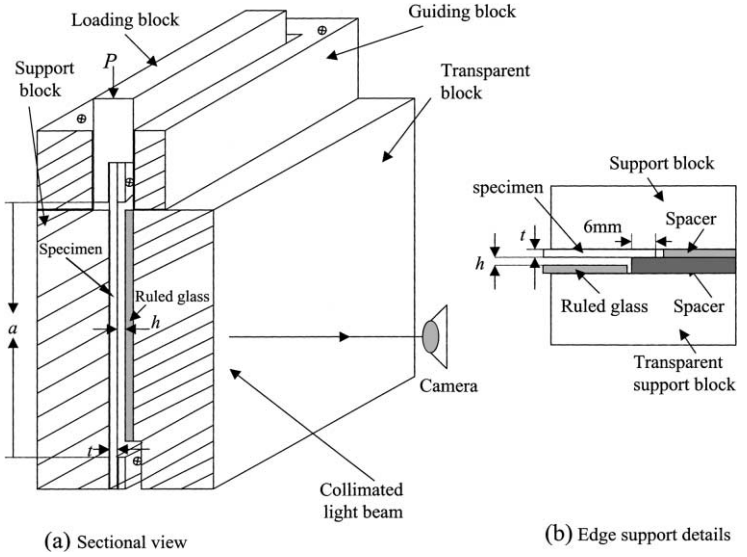

Fig. 4. Schematics of the test fixture and test panel for a bilaterally constrained plate.

Figs. 5–8 show four moire sequences exposing the effects of plate aspect ratio, confinement distance and load level. The normalized displacement (K) is noted in each print; as indicated earlier, in all these configurations the theoretical buckling load is $K \approx 10$, irrespective of R. In all cases, $(t, b) = (0.5, 76.2)$ mm; this is except for Fig. 5, where $t = 0.7$ mm. A summary of the main features follows.

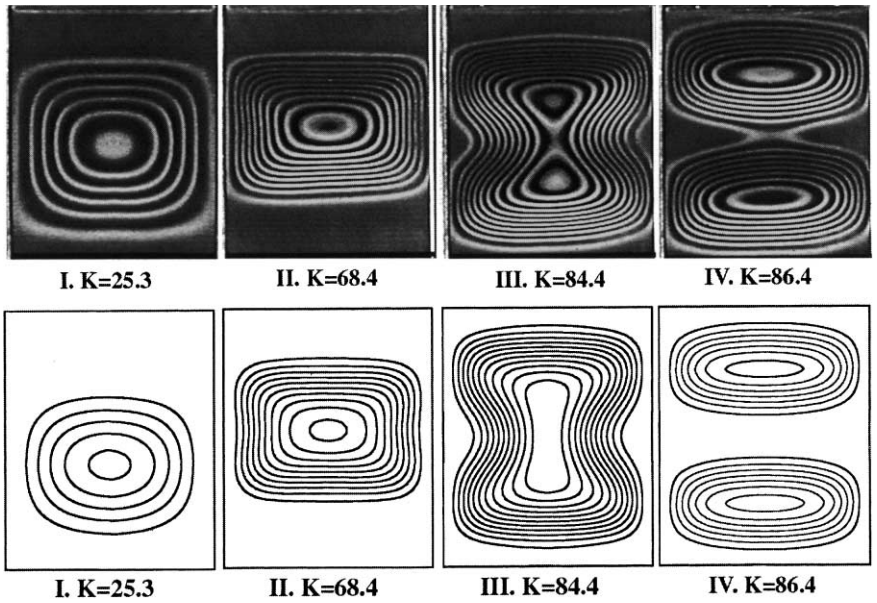

Fig. 5. Outward displacement contours at increasing normalized axial displacement for unilaterally constrained plate ($h \to \infty$), $t = 0.7$ mm, $b = 76.2$ mm, $R = 1.2$, fringe constant $f = 0.3$ mm; upper sequence corresponds to experiments, lower sequence is FEM prediction based on the same load levels as above.

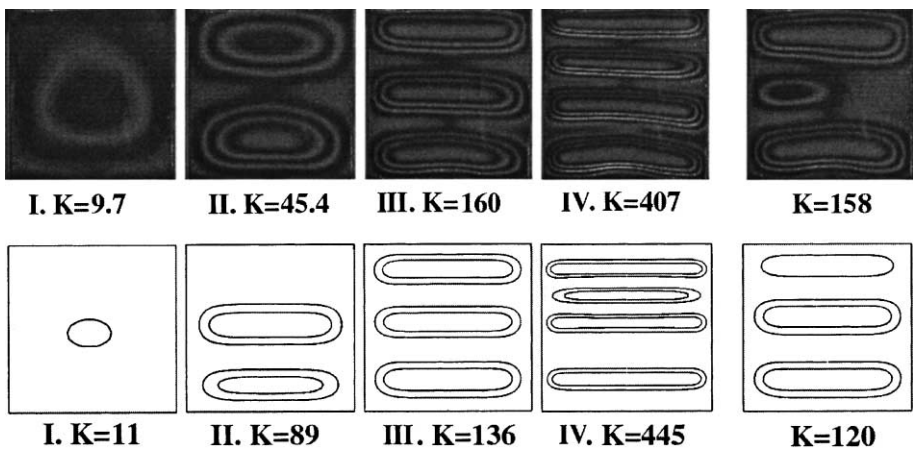

Fig. 6. Outward displacement contours for bilaterally constrained plate, $t = 0.5$ mm, $b = 76.2$ mm, $R = 1$, $h = 0.8$ mm, $f = 0.3$ mm; upper sequence corresponds to experiments while lower sequence to FEM predictions. Each of the prints I–IV corresponds to just after the completion of buckling mode transition; the far-right frame in each sequence shows the process of transition from 2 to 3 buckles.

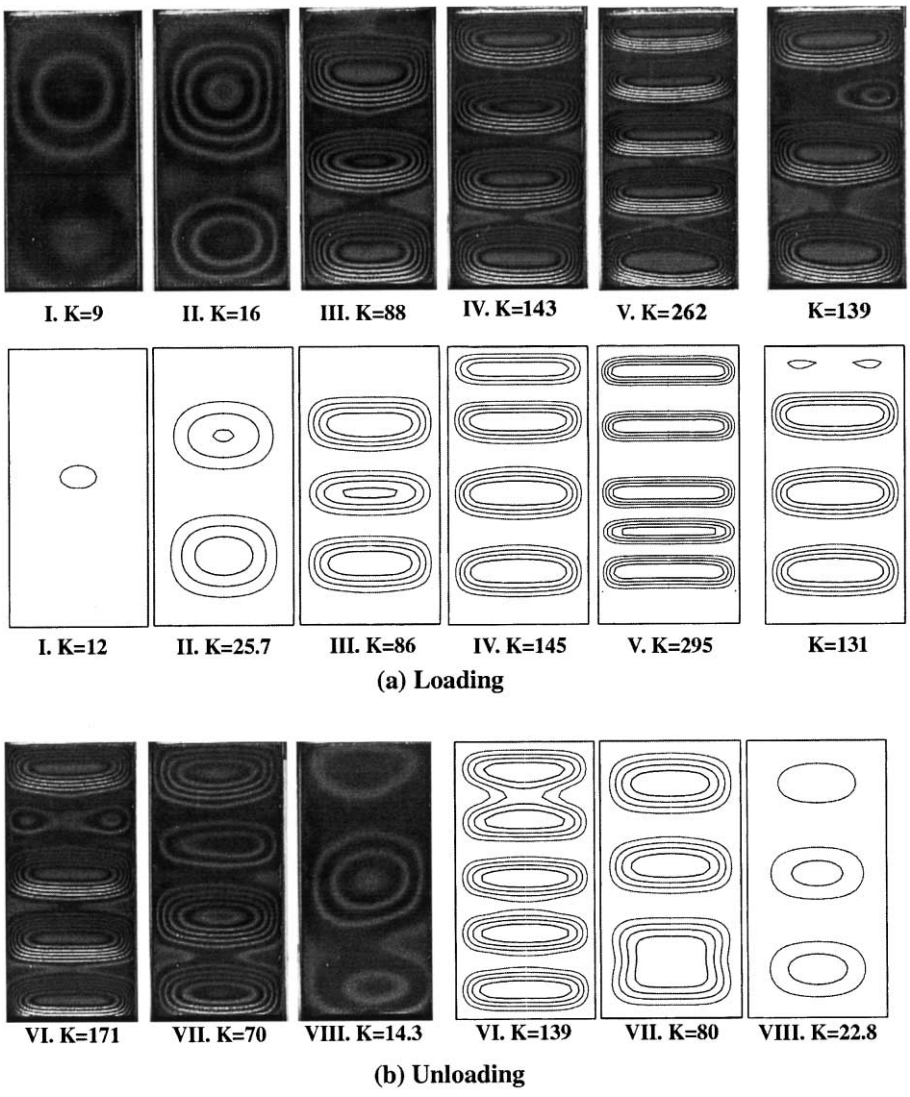

Fig. 7. (a) As in Fig. 6, $t = 0.5$ mm, $b = 76.2$ mm, $R = 2$, $h = 1.5$ mm, $f = 0.3$ mm; the far-right frame in each sequence shows the process of transition from 3 to 4 buckles. (b) Unloading history for the plate in (a).

Fig. 5—This sequence exemplifies the unilateral constraint case ($h \to \infty$) for small aspect ratio ($R = 1.2$). Notable events are the onset of secondary buckling which occurs within the bulge region, near its vertical edges (II), the final stage of bulge collapse (III), and the splitting of the bulge into two separate bulges (IV). Note the asymmetry of the deformation (II), and the mobility of the buckle during the loading. It is interesting to note that this mode transition process is similar to that observed in hat-stiffened, laterally unrestrained plates (Knight and Starnes, 1988; Falzon and Steven, 1997), or to circumferential buckling in circular plates (Nilsson and Giannakopoulos, 1995).

Fig. 6—$R = 1$, $h = 0.8$ mm. Each frame in this sequence corresponds to just after the completion of buckling mode transition, i.e. from 0 to 1 (I), 1 to 2 (II), 2 to 3 (III) and 3 to 4 (IV) buckles. As shown by the

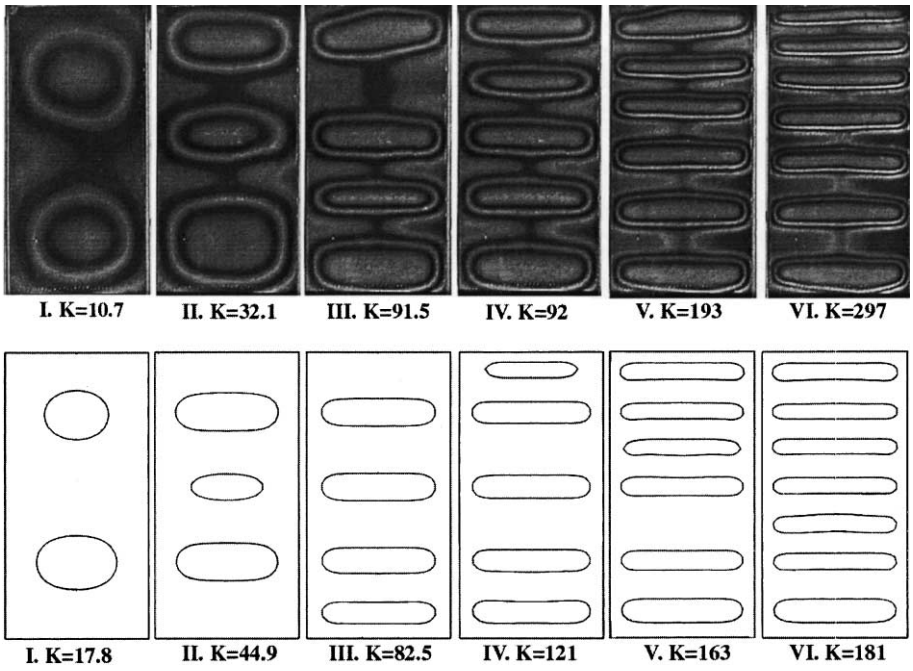

Fig. 8. As in Fig. 7a except $h = 0.5$ mm. Note that the formation of the first buckle is not shown.

print on the far right ($K = 158$), the transition (e.g. from 2 to 3 buckles) evolves from the local buckling of the contact region formed between adjacent buckles. Comparison with Fig. 5 shows that the introduction of a second lateral constraint significantly alters the deformation process, notably in the generation of more buckles within the span of the plate, and also in the suppression of circumferential type instability in favor of contact type instability. Another striking feature in this sequence is that the deformation pattern becomes essentially one dimensional once contact with the two walls is established.

Fig. 7—$R = 2$, $h = 1.5$ mm. Shown are loading (a) and unloading (b) histories. Loading: Interaction of the buckle with the second constraining surface is reached only after the second buckle emerges. The position of the first buckle (I) seems highly asymmetric, in consistency with earlier discussions. The rest of the behavior is similar to Fig. 6, including the process of buckling mode transition (right side print, $K = 139$). Unloading: Each of the prints VI–VIII corresponds just before the transition to a lower buckling mode. The associated loads ($K = 171$, 70, 14.3) are well less than their respective loading counterparts ($K = 262$, 143, 88), indicating a pronounced hysteresis.

Fig. 8—$R = 2$, $h = 0.5$ mm. The deformation sequence is similar to that for the plate with the larger gap (Fig. 7a), except that more buckles are generated for a given edge displacement. Also, interaction of the plate with the opposing surface occurs prior to the emergence of the second buckle (I).

Several trends are apparent from these and similar tests. (1) The bulges are generally asymmetric, with their position changing with load. (2) Local instability is the precursor to buckling mode transition. This instability conclusively initiates from a contact region, near the edges of the plate, where the stresses apparently are the largest. (3) The plate response is initially similar to that for the unilaterally constrained case, but as the interaction of the plate with the opposing wall progresses, the deformation pattern tends to resemble that of the bilaterally constrained column.

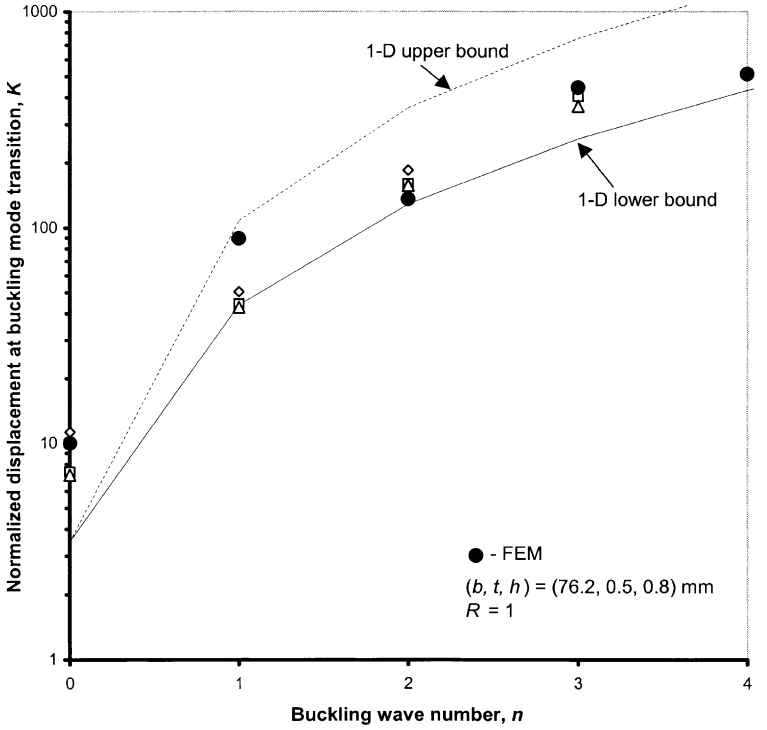

Fig. 9. The normalized axial displacement just after the completion of buckling mode transition, from n to $n+1$ buckles, as a function of n for a bilaterally constrained plate (case study of Fig. 6); $(t, b, h) = (0.5, 76.2, 0.8)$ mm, $R = 1$. Open symbols are from experiments and filled circles are FEM predictions. Lower and upper bounds correspond to Eq. (13), with K relating to $\overline{\Delta}$ through Eq. (14).

Figs. 9–11 (open symbols) show the variation of the load at the transition from n to $n+1$ buckles with wave number n for the three case studies depicted in Figs. 6–8; different symbols for a given n correspond to repeating tests on the same specimen. The data for a given buckling mode exhibit a significant scatter among repeating tests. The snapping loads monotonically increase with n, with the first buckle occurring reasonably close to the theoretical value $K = 10$. The rather abrupt changes in the plate response for small values of n that is seen in these figures is caused by the initial interaction of the plate surface with the opposing plane. Fig. 12 is a composite plot showing the dependence of the axial displacement at the time of transition from 1 to 2 buckles or from 3 to 4 buckles, normalized as for the 1-D configuration, on the normalized confinement distance h/t. The results, which include data from the tests of Figs. 9–11 as well as other plate geometry, seem to obey reasonably well this 1-D type normalization.

In attempting to quantify the rather complex behavior observed for the bilaterally constrained plate, the loading history can be broken into two parts. In the early buckling stage, no contact between the plate and the opposing rigid plane occur, which reduces the problem to that of a unilaterally constrained plate. In this case, it was shown that the distribution of contact zones within the plate is not arbitrary, as for the 1-D case (Section 2), but rather it is dictated by a minimum strain energy requirement. The latter entails an extreme form of asymmetry in the plate deformation (Chai, 2000), which is consistent with the observed behavior (e.g. print I of Fig. 7). Once contact with both confining walls is established, the plate deformation tends to resemble that of the bilaterally constrained column. It is this feature that has motivated the development of the 1-D model (Section 2). Figs. 9–12 show the 1-D bounds from Eq. (13) (solid and dotted curves),

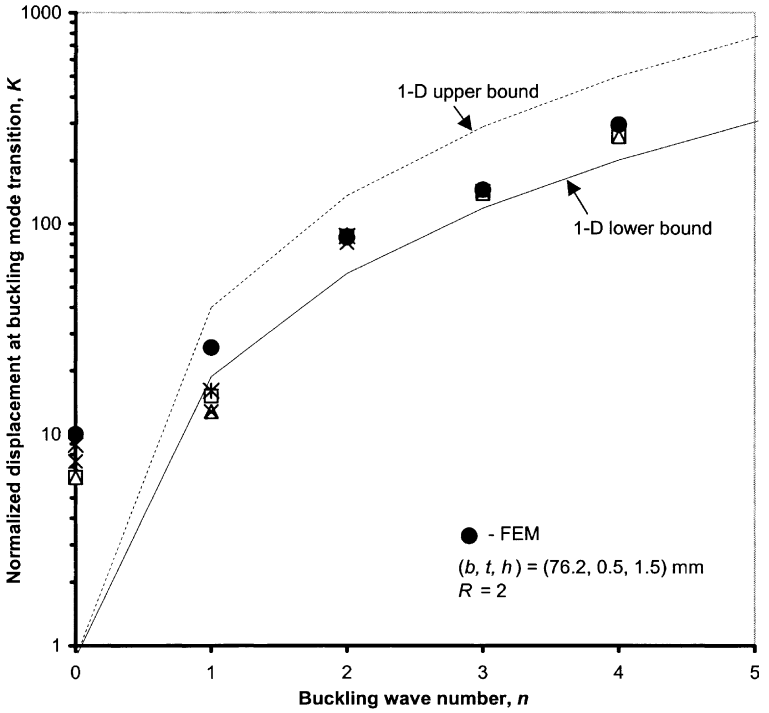

Fig. 10. The normalized axial displacement for buckling mode transition, from n to $n+1$ buckles, as a function of n for a bilaterally constrained plate (case study of Fig. 7); $(t, b, h) = (0.5, 76.2, 1.5)$ mm, $R = 2$. Open symbols are from experiments and filled circles are FEM predictions. Lower and upper bounds correspond to Eq. (13), with K relating to $\overline{\Delta}$ through Eq. (14).

expressed in terms of K in the case of Figs. 9–11 using Eq. (14). Except for small values of n (i.e. 1 or 2), the plate results seem to be well contained within the 1-D bounds, in consistency with the above discussion.

3.2. Finite element analysis

A large-strain, commercial finite element code with built-in contact algorithm is employed (Ansys, Version 5.4). Eight-node isoparametric plate element (Shell 63) and a three-dimensional contact element (Contact 49) are used. Friction between the plate and the two lateral supports is modeled as a Coulomb friction with a coefficient μ, taken as 0.35 in this study. In consistency with the tests, the outward deflection, w, and the plate rotation, $\mathrm{d}w/\mathrm{d}l$, where l denotes the normal to the plate boundary, are assumed zero along all four edges of the plate. Also, the in-plane displacements on the lower edge, and the horizontal displacement on the upper edge, are assumed zero. The upper edge is given a uniform downward displacement that is applied in load steps. A small initial outward displacement, placed a distance $R_0/2$ from the lower edge of the plate, is implemented in order to help obtain a smooth transition into the buckling regime; this auxiliary displacement is removed once buckling takes place. To take advantage of symmetry, only half of the plate area is modeled. A systematic mesh refinement study shows that as many as 1250 elements are necessary to insure convergence of the post-buckling solution over the range of parameters studied.

Figs. 5–8 show sequences of displacement contours analogous to the experimental case studies depicted in the upper part of these figures. Each load in the FEM sequence of Fig. 5 is numerically identical to its experimental counterparts. In the case of Figs. 6–8, the loading in each frame corresponds to the buckling

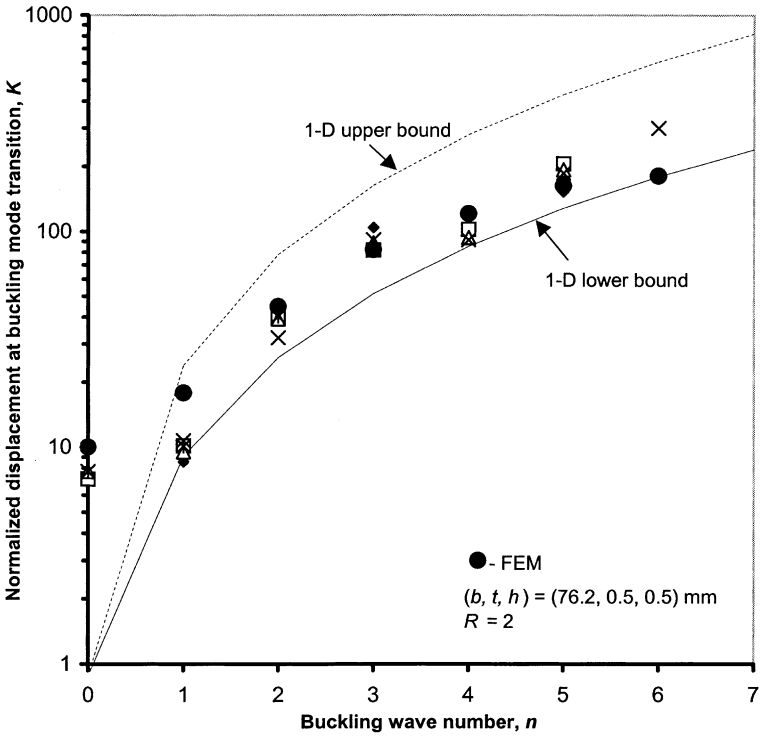

Fig. 11. The normalized axial displacement for buckling mode transition, from n to $n+1$ buckles, as a function of n for a bilaterally constrained plate (case study of Fig. 8); $(t, b, h) = (0.5, 76.2, 0.5)$ mm, $R = 2$. Open symbols are from experiments and filled circles are FEM predictions. Lower and upper bounds correspond to Eq. (13), with K relating to $\overline{\Delta}$ through Eq. (14).

mode transition load, as determined from visual inspection of the FEM deformation pattern. It is evident that the FEM results generally well resemble the tests, in the appearance and level of deformation as well as in identifying local instability in a contact zone as the precursor for buckling mode transition. The FEM predictions for the buckling mode transition loads are depicted in Figs. 9–11 as solid circles. As shown, the FEM values are much similar to their experimental counterparts.

The load bearing capacity of the buckled plate is an important design parameter. Fig. 13 (solid line) shows FEM-generated load histories (i.e. full loading–unloading cycle) for the case study discussed in Fig. 7 ($R = 2$, $h = 1.5$ mm). The axial force applied to the specimen edge, P, is normalized by P_0, the trivial solution corresponding to the unbuckled state, given as $btE\Delta/a$, while the axial displacement is normalized so as to render the horizontal coordinate as axial strain in the unbuckled state. The loading segment exhibits a pronounced jerky trace resulting from plate snapping. The unloading segment exhibits a large hysteresis effect, which is elastic in nature. A similar observation was also made in a study of unilaterally constrained rods (Suryanarayana and McCann, 1995). Comparison with the frictionless case ($\mu = 0$), shown in this figure as a dotted curve, indicates that friction is significant only after the formation of several buckles, causing some reduction in the axial force during the loading phase. The energy absorption capacity of the bilaterally constrained plate can be appreciated from a comparison with the extreme case of unilateral support ($h \to \infty$, dashed dot line). Reducing the confinement distance tends to increase the normalized edge force, up to unity in the limit $h = 0$ (horizontal dash—triple-dot line). However, decreasing h as a means for increasing energy absorption should not be overdone in order to avoid material failure or fracture.

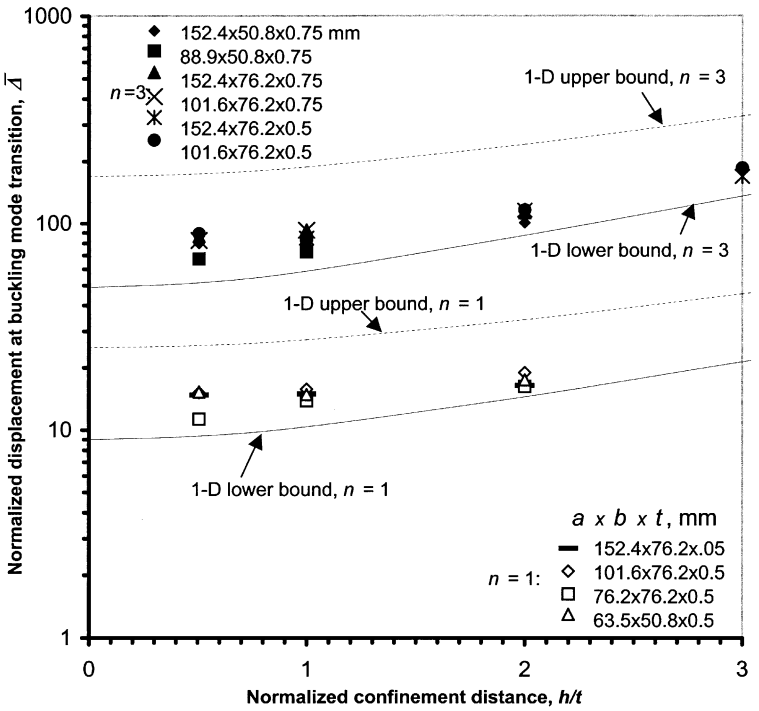

Fig. 12. Experimental composite plots showing normalized axial displacement at buckling mode transition, from $n = 1$ to $n = 2$ buckles (lower data), and from $n = 3$ to $n = 4$ buckles (upper data), as a function of normalized confinement distance for bilaterally constrained plates. As noted in the figure, different symbols correspond to different plate geometry. Lower and upper bounds correspond to Eq. (13).

4. Summary and conclusions

The post-buckling response of bilaterally constrained columns and plates under monotonically increasing edge displacement is studied experimentally and analytically. The tests show that the interaction of the buckled plate with the adjoining rigid substrates leads to a unique deformation pattern, characterized by buckled portions and flattened zones within the plate, and the rapid transition of the buckling waveform to new equilibrium states following a gradual evolution of secondary buckles which originate from contact regions. The specifics strongly depend on the plate aspect ratio, the confinement distance and the loading level. The response of the bilaterally constrained plate can be viewed as a hybrid of the unilaterally constrained plate and the bilaterally constrained column, with the former dominating in the early buckling stages while the latter in the post-buckling regime, once contact with the two confining walls is established. The buckling mode transition loads, while exhibiting a degree of statistical scatter, increase with the confinement distance, especially when h/t is increased from unity.

A simple analytical model, based on the linear theory of beams, is developed for predicting the onset of buckling mode transition in a bilaterally constrained column. Upper and lower bounds predicted by this analysis are substantiated by the 1-D experimental data. Application of this model to the plate problem shows similar success provided the interaction of the plate with both of the confining walls is already established. A geometrically non-linear FEM scheme incorporating frictional contact is used to elucidate the plate response. The analysis well duplicates the main sequence of events observed in the tests as well as the critical loads for mode transition.

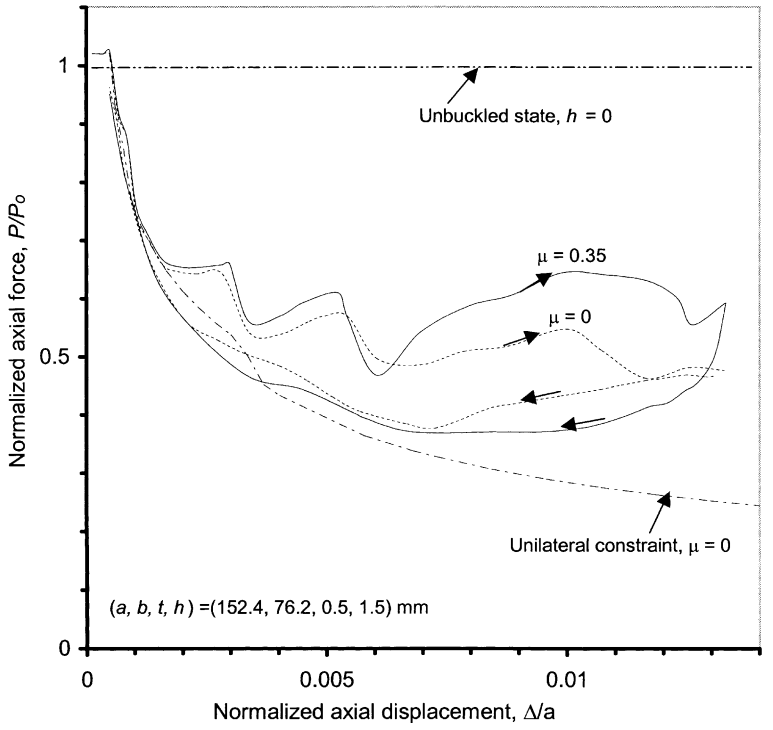

Fig. 13. FEM loading histories for bilaterally constrained plate, $(t, b, h) = (0.5, 76.2, 1.5)$ mm, $R = 2$. P is the axial force applied to the specimen edge, P_0 corresponds to the unbuckled state. Solid and dotted curves correspond to a friction coefficient $\mu = 0.35$ and $\mu = 0$, respectively. Also shown is the result for a unilateral constraint plate ($h \to \infty$).

The present work may bear on a variety of engineering applications. The relatively large area under the load vs. end shortening curve seem to offer a viable source for energy absorption. A laminated form of this unit structure may be appealing from crashworthiness viewpoint. In such applications, incorporation of plasticity into the analysis would be useful.

Acknowledgements

The author thanks Mr. David Armoni for his help in constructing the test fixtures and test samples.

References

Adan, N., Sheinman, I., Altus, E., 1994. Post-buckling behavior of beams under contact constraints. Journal of Applied Mechanics 61, 764–772.

Chai, H., 1990a. Three-dimensional analysis of thin-film debonding. International Journal of Fracture 46, 237–256.

Chai, H., 1990b. Buckling and post-buckling behavior of elliptical plates: Part II. Results. Journal of Applied Mechanics 57, 989–994.

Chai, H., 1998. The post-buckling behavior of a bilaterally constrained column. Journal of the Mechanics and Physics of Solids 46, 1155–1181.

Chai, H., 2000. Contact buckling and post-buckling behavior of thin rectangular plates. Journal of the Mechanics and Physics of Solids 49, 203–230.

Chateau, X., Nguyen, Q.S., 1991. Buckling of elastic structures in unilateral contact with or without friction. European Journal of Mechanics, A/Solids 1, 71–89.
Comiez, J.M., Waas, A.M., Shahwan, K.W., 1995. Delamination buckling; experiment and analysis. International Journal of Solids and Structures 32, 767–782.
Falzon, B.G., Steven, G.P., 1997. Buckling mode transition in hat-stiffened composite panels loaded in uniaxial compression. Composite Structures 37, 253–267.
Gupta, N.K., Prasad, E., Gupta, S.K., 1999. Axial compression of metallic spherical shells between rigid plates. Thin-Walled Structures 34, 21–41.
Holmes, P., Domokos, G., Schmitt, J., Szeber'enyi, I., 1999. Constrained Euler buckling: an interplay of computation and analysis. Computer Methods in Applied Mechanics and Mechanical Engineering 170, 175–207.
Jones, R., Broughton, W., Mousley, R.F., Potter, R.T., 1985. Compression failure of damaged graphite epoxy laminates. Composite Structures, Elsevier Applied Science Publishers, 167–185.
Keller, H.B., Reiss, E.L., 1958. Non-linear bending and buckling of circular plates. In: Proceedings of the 3rd U.S. National Congress of Applied Mechanics and Engineering, pp. 375–385.
Kim, J.B., Yoon, J.W., Yang, D.Y., 2000. Wrinkling initiation and growth in modified Yoshida buckling test: finite element analysis and experimental comparison. International Journal of Mechanical Sciences 42, 1683–1714.
Knight Jr., N.F., Starnes Jr., J.H., 1988. Post-buckling behavior of selected curved stiffened graphite-epoxy panels loaded in axial compression. AIAA Journal 26 (3), 344–352.
Kobayashi, A.S., 1993. Handbook on Experimental Mechanics, second ed. Society for Experimental Mechanics.
Kublanov, L.B., Bottega, W.J., 1995. On pressing a buckled film. Applied Mathematical Modeling 19, 499–507.
Levy, S., 1942. Buckling of rectangular plates with built-in edges. Journal of Applied Mechanics, June, A171–A174.
Nakamura, T., Uetani, K., 1979. The secondary buckling and post-secondary-buckling behaviours of rectangular plates. International Journal of Mechanical Sciences 21, 265–286.
Nilsson, K.L., Giannakopoulos, A.E., 1995. A finite element analysis of configurational stability and finite growth of buckling driven delamination. Journal of the Mechanics and Physics of Solids 43, 1983–2021.
Ohatake, K., Oden, J.T., Kikuchi, N., 1980. Analysis of certain unilateral problems in von Karman plate theory by a penalty method – Part 2, Approximation and numerical analysis. Computer Methods in Applied Mechanics and Engineering 24, 317–337.
Patel, P., Nordstrand, T., Carlsson, L.A., 1997. Local buckling of collapse of corrugated board under biaxial stress. Composite Structures 39, 93–110.
Roger Ku, C.-.P., Heshmat, H., 1993. Compliant foil bearing structural stiffness analysis – Part II: Experimental investigation. Journal of Tribology 115, 364–369.
Sekine, H., Nu, H., Kouchakzadeh, M.A., 2000. Buckling analysis of elliptically delaminated composite laminates with consideration of partial closure of delamination. Journal of Composite Materials 34, 551–573.
Shahwan, K.W., Waas, A.M., 1997. Non-self-similar decohesion along a finite interface of unilaterally constrained delaminations. Proceedings of the Royal Society of London A 453, 515–550.
Shahwan, K.W., Waas, A.M., 1998a. Buckling of unilaterally constrained infinite plates. Journal of Engineering Mechanics (Feb.), 127–136.
Shahwan, K.W., Waas, A.M., 1998b. Buckling of unilaterally constrained plates: application to the study of delaminations in layered structures. Journal of the Franklin Institute 335B (6), 1009–1039.
Siede, P., 1958. Compressive buckling of a long simply supported plate on an elastic foundation. Journal of the Aeronautical Sciences (June), 382–394.
Stein, M., 1959. Loads and deformation of buckled rectangular plates. NASA Technical Report R-40.
Suryanarayana, P.V.R., McCann, R.C., 1995. An experimental study of buckling and post-buckling of laterally constrained rods. Journal of Energy Resources Technology 117, 115–124.
Urbanik, T.J., 1996. Machine direction strength theory of corrugated fiberboard. Journal of Composites Technology & Research 18, 80–88.
Wright, H.D., 1995. Local instability of filled and encased steel sections. Journal of Structural Engineering 121, 1382–1387.
Wu, J., Juvkam-Wold, H.C., 1995. Buckling and lockup of tubulars in inclined wellbores. Journal of Applied Mechanics 117, 208–213.